

RESEARCH

Open Access



Disulfidptosis-related signature predicts prognosis and characterizes the immune microenvironment in hepatocellular carcinoma

Jun Tang^{1,2†}, Xintong Peng^{1,2†}, Desheng Xiao⁴, Shuang Liu⁵, Yongguang Tao^{1,2,3,4*} and Long Shu^{1,2*}

Abstract

Background Disulfidptosis is a type of programmed cell death caused by excessive cysteine-induced disulfide bond denaturation leading to actin collapse. Liver cancer has a poor prognosis and requires more effective intervention strategies. Currently, the prognostic and therapeutic value of disulfidptosis in liver cancer is not clear.

Methods We investigated the features of 16 disulfidptosis-related genes (DRGs) of HCC patients in the TCGA and classified the patients into two disulfidptosis pattern clusters by consensus clustering analysis. Then, we constructed a prognostic model using LASSO Cox regression. Next, the microenvironment and drug sensitivity were evaluated. Finally, we used qPCR and functional analysis to verify the reliability of hub DRGs.

Results Most of the DRGs showed significantly higher expression in cancer tissues than in adjacent tissues. Our prognostic model, the DRG score, can well predict the survival of HCC patients. There were significant differences in survival, features of the microenvironment, effects of immunotherapy, and drug sensitivity between the high- and low-DRG score groups. Ultimately, we demonstrated that a few hub DRGs have differential mRNA expression between liver cancer cells and normal cells and that the protective gene *LCAT* can inhibit liver cancer metastasis in vitro.

Conclusion We established a novel risk model based on DRG scores to predict HCC patient prognosis, drug sensitivity and immunotherapy efficacy, which provides new insight into the relationship between disulfidptosis and HCC and provides valuable assistance for the personalized treatment of HCC.

Keywords Disulfidptosis, Hepatocellular carcinoma, Immune microenvironment, Prognostic model

[†]Jun Tang and XinTong Peng have contributed equally to this work and share the first authorship.

*Correspondence:
Yongguang Tao
taoyong@csu.edu.cn
Long Shu
22022039@csu.edu.cn

¹ Key Laboratory of Carcinogenesis and Cancer Invasion (Ministry of Education), NHC Key Laboratory of Carcinogenesis (Central South University), Cancer Research Institute and School of Basic Medicine, Central South University, Changsha 410078, Hunan, China

² Hunan Key Laboratory of Cancer Metabolism, Hunan Cancer Hospital and The Affiliated Cancer Hospital of Xiangya School of Medicine, Central South University, Changsha 410078, Hunan, China

³ Department of Thoracic Surgery, Hunan Key Laboratory of Early Diagnosis and Precision Therapy in Lung Cancer, Second Xiangya Hospital, Central South University, Changsha 410011, China

⁴ Department of Pathology, Xiangya Hospital, Central South University, Changsha 410008, Hunan, China

⁵ Department of Oncology, Institute of Medical Sciences, National Clinical Research Center for Geriatric Disorders, Xiangya Hospital, Central South University, Changsha 410008, Hunan, China



Introduction

Worldwide, hepatocellular carcinomas account for 80–90% of liver cancer cases, making it one of the most lethal tumors. The factors of liver cancer include aflatoxin, viral infections (HBV and HCV), metabolic alteration (alcoholic steatohepatitis, nonalcoholic steatohepatitis), obesity, smoking, etc. [1, 2]. Currently, the majority of patients with liver cancer receive their diagnosis at an advanced stage, and they typically have a dismal prognosis. In actuality, few patients are eligible for surgical procedures, and prolonged chemotherapy use increases the risk of toxicity or drug resistance. In addition, only 20% of patients are candidates for treatment with immune checkpoint inhibitors (ICPs). Therefore, it is imperative and urgent to continue researching possible targets for the treatment of liver cancer treatment [3, 4].

Disulfidptosis is a recently discovered form of cell death. It occurs in cells with high expression of SLC7A11, in which glucose depletion leads to a reduction in intracellular NADPH production. This results in the accumulation of cysteine, which causes abnormal accumulation of disulfides and ultimately leading to cell death through targeting of the actin cytoskeleton [5, 6]. Importantly, GLUT inhibitors can induce disulfidptosis in SLC7A11^{high} tumor cells, inhibiting tumor growth both in vitro and in vivo. The mechanism of disulfidptosis provides interesting potential targets for cancer treatment. Furthermore, metastatic cancer cells have more lamellipodia and invasive protrusions, suggesting that they may be more sensitive to disulfidptosis [7]. Targeting metabolic reprogramming is one of the strategies in cancer treatment, and the study of disulfidptosis, as a novel form of metabolism-related cell death, offers new insights for cancer therapy and clinical translation [8, 9].

Glucose metabolism is important for tumor growth and progression, and glycogen accumulation is an important event in inducing liver tumor initiation [10]. Furthermore, prohibiting tumor malignancy and reducing the incidence of hepatic carcinoma by removing excess glycogen from the body is an efficient approach. Notably, disulfidptosis is a novel type of programmed cell death (PCD), which is caused by actin cytoskeleton network collapse due to bond abnormalities abnormality under glucose conditions. Thus, disulfidptosis may be strongly associated with the retardation of the malignant progression of liver cancer. However, the molecular mechanism by which disulfidptosis suppresses liver cancer is currently unclear.

In this study, we explored the expression profiles of 16 DRGs and related features in HCC. A disulfidptosis-related risk model based on DRG scores was established to predict HCC patient features and prognosis. We also investigated the tumor microenvironment

(TME) infiltration, drug sensitivity and immunotherapy response in different DRG score groups of HCC patients. Additionally, we revealed the role of LCAT induced disulfidptosis in the progression of liver cancer, providing new insight into liver cancer treatment via targeted disulfidptosis. The overall experimental design and major steps are could be shown in Fig. 1.

Materials and methods

Patient data source

The Log₂ (RSEM + 1) normalized gene expression data, gene copy number variation data estimated using the GISTIC2 method, and corresponding clinical data of the TCGA-LIHC cohort were downloaded from UCSC Xena (<https://xenabrowser.net/>). The testing cohort International Cancer Genome Consortium (ICGC-LIRI-JP) for liver cancer was downloaded from the ICGC Data Portal (<https://dcc.icgc.org/>). We further included patients with OS time greater than 0, complete survival status information, and comprehensive clinical and pathological data. Table 1 presents the age, sex, pathological stage, and survival information of the included patients. The copy number variation of genes was visualized by the “RCircos” package.

Clustering analysis for disulfidptosis-related genes

Sixteen disulfidptosis-related genes [including 4 confirmed suppressors of disulfidptosis (NCKAP1, RPN1, SLC3A2 and SLC7A11) and 12 potential synergistic of disulfidptosis (PPM1F, CNOT1, NDUFC1, NDUFA11, NDUFA10, LRPPRC, NUBPL, NDUFS2, GYS1, EPAS1, NDUFS1 and OXSM)] were obtained from the previous studies of Liu et al. in 2023 [5]. These DRGs can be seen in Additional file 2: Table S1. We conducted the consensus clustering analysis using the ConsensusClusterPlus R package, (parameters of reps=1000), to assess the disulfidptosis status and DRG cluster clusters of HCC patients in the TCGA-LIHC cohort. We select a suitable parameter for clusters through the CDF curve. Then, the patient OS time was determined through Kaplan–Meier (K-M) analysis using the “survival” and “survminer” packages.

Identification of DEGs and GSEA

Differential gene expression (DEGs) analysis between two disulfidptosis regulated clusters was performed using an empirical Bayesian algorithm using the “limma” R package and DEGs were given a significance threshold of $|\log_2(\text{FoldChange})| > 1$ and an adjusted P-value of 0.05. Applying the “clusterProfiler” packages, gene set enrichment analysis (GSEA) and gene ontology (GO) enrichment analyses were carried out to study the biological activities of two disulfidptosis regulated clusters

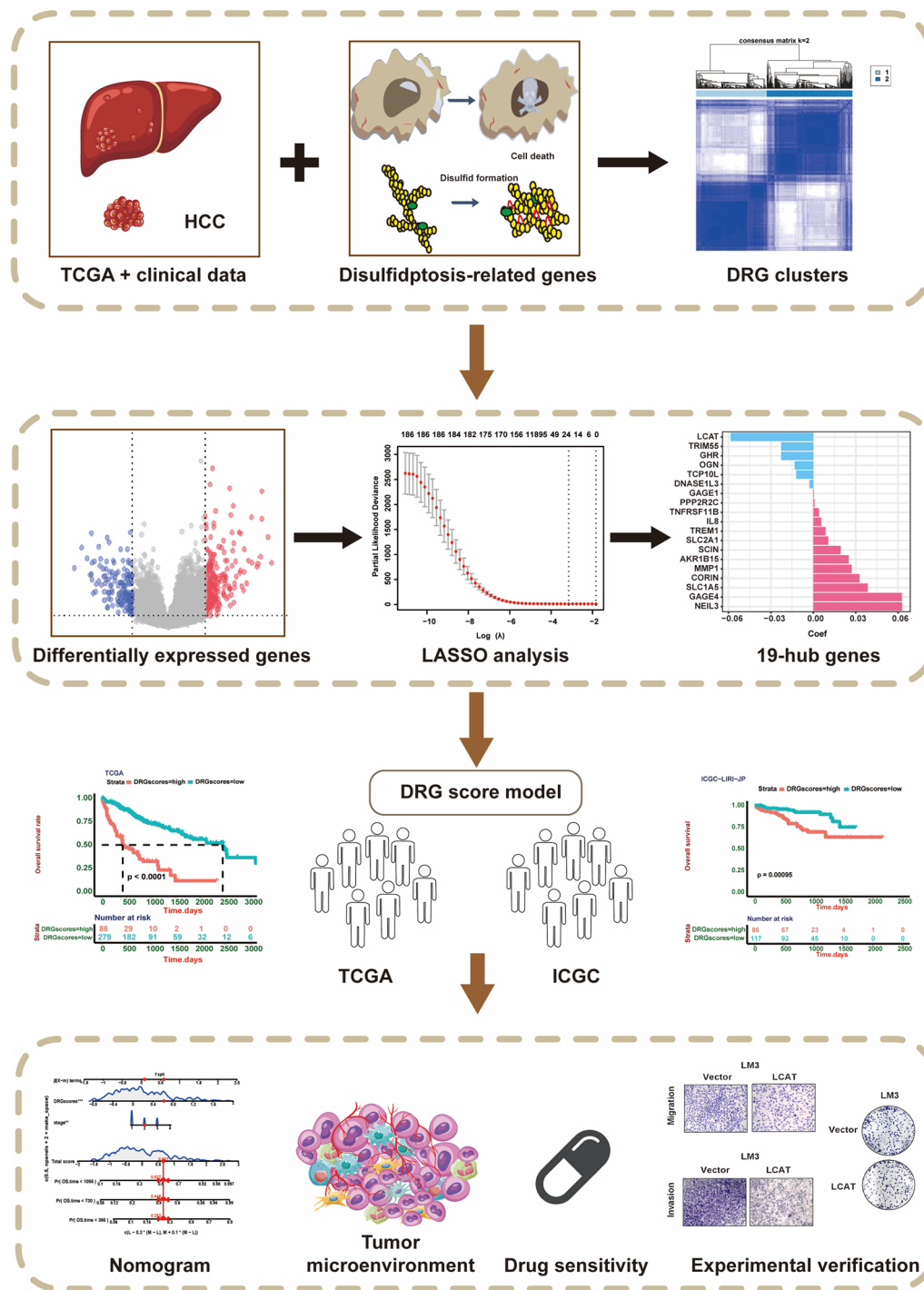


Fig. 1 The overall experimental design and major steps of our study. We first investigated the expression of 16 disulfidptosis-related genes in HCC patients in the TCGA-LIHC cohort and categorized the HCC patients into two DRG clusters based on the expression of those genes. Subsequently, we selected DEGs with prognostic significance between DRG clusters for LASSO analysis. In total, 19 hub genes were selected for the construction of the DRG score model in the TCGA cohort, which was validated in an external ICGC cohort. Then, we developed a nomogram based on our model and assessed immune infiltration and drug sensitivity in HCC patients. Finally, through experimental validation, we confirmed the anticancer role of the hub gene LCAT in liver cancer and explored its potential association with disulfidptosis-related death. *DRG* Disulfidptosis-related gene, *HCC* hepatocellular carcinoma, *LASSO* least absolute shrinkage and selection operator, *DEG* differentially expressed gene

Table 1 Clinical characteristics of HCC patients from TCGA and ICGC database

	TCGA	ICGC	Overall
Age (years)			
Mean (SD)	59.6 (13.4)	67.0 (10.2)	62.3 (12.8)
Median	61.0	69.0	64.0
Gender			
Female	119 (32.6%)	50 (24.6%)	169 (29.8%)
Male	246 (67.4%)	153 (75.4%)	399 (70.2%)
TNM stage			
I	170 (46.6%)	33 (16.3%)	203 (35.7%)
II	84 (23.0%)	96 (47.3%)	180 (31.7%)
III	83 (22.7%)	59 (29.1%)	142 (25.0%)
IV	4 (1.1%)	15 (7.4%)	19 (3.3%)
Unknow	24 (6.6%)	0 (0%)	24 (4.2%)
Survival status			
Alive	234(64.1%)	168 (82.8%)	402 (70.8%)
Dead	130 (35.6%)	35 (17.2%)	165 (29.0%)
Not reported	1 (0.3%)	0 (0%)	1 (0.2%)
OS time (days)			
Mean (SD)	813 (726)	828(417)	818 (633)
Median	596	810	661

HCC hepatocellular carcinoma, TCGA the cancer genome atlas, ICGC international cancer genome consortium

[11]. Annotation files for GO, the Kyoto Encyclopedia of Genes and Genomes (KEGG), and hallmark pathways were downloaded from the GSEA website (<http://www.gsea-msigdb.org/gsea/index.jsp>).

Construction and validation of prediction models

The univariate Cox proportional hazards regression survival analysis was performed via the “survival” R package to filter prognostic genes as in the TCGA-LIHC cohort based on the DEGs between two disulfidptosis regulated clusters. The prognostic genes were then further filtered to identify hub DRGs genes using the least absolute shrinkage and selection operation (LASSO) and tenfold cross validation using the “glmnet” R package. The sum of the expression value and weight coefficients of the hub genes was then used to calculate the DRG scores for each sample:

$$\text{DRGscores} = \sum_{k=1}^n \binom{n}{k} \text{LASSO_coef}^k * \text{Expression}^k$$

To evaluate the survival probabilities between the two DRG score groups in the TCGA training cohort, a Kaplan–Meier (K–M) analysis was conducted using the “survival” and “survminer” packages. The area under the curve (AUC) was calculated using the “timeROC” package, which also performed receiver operating

characteristic (ROC) analysis across 1, 3, and 5 years. Similarly, K–M survival curves and ROC curves were generated for the ICGC-LIRI-JP testing cohort. Then, using clinical traits and DRG scores, multivariate Cox proportional-hazards regression was used to identify the independent predictors of HCC prognosis. Finally, using the “rms” R package, the stage and DRG scores served as independent predictors to generate a nomogram for clinical application. [12]. To assess the nomogram model, the “ggDCA” R package implemented the decision curve analysis (DCA).

Immune feature evaluation of DRG scores

Each HCC patient in the TCGA-LIHC cohort was assigned an immune score, stromal score, and an ESTIMATE score using the ESTIMATE method. The infiltration score of 23 human immune cells in each HCC patient was calculated via the CIBERSORT algorithm [13]. Additionally, Spearman correlation analysis was used to determine whether immune checkpoint genes and DRG scores in HCC patients were correlated.

Analysis of drug susceptibility and immunotherapy response

For HCC patients in the TCGA-LIHC cohort, the Tumor Immune Dysfunction and Exclusion (TIDE) algorithm was used to forecast the immunotherapy response (<http://tide.dfci.harvard.edu>) [13]. The “oncoPredict” package was used to calculate the half-inhibitory concentration (IC50) values for 198 medicines, including cancer treatment and medications specifically for HCC. [14].

scRNA-seq data analysis

Single-cell data of seven tumors of untreated HBV-related hepatocellular carcinoma (HCC) patients were downloaded from the GEO website (GSE202642) [15]. The “Seurat” R package was used for standardizing the single-cell analysis workflow. Cells expressing a minimum of 200 genes with mitochondrial percentage less than 10% were selected, followed by normalization and scaling. Subsequently, the RunPCA function was employed to perform principal component analysis (PCA), and the top 15 PCs were chosen for uniform manifold approximation and projection (UMAP) reduction. Cell type annotations were performed based on the marker genes of the major cell clusters. Finally, the AddModuleScore function was used to generate the DRG signature at the single-cell level.

Cell culture

The Cancer Research Institute of Central South University provided HepG2, L-02, SMMC-7721, HCCLM3 and Hep3B cells, as well as 293 T cells. All cell lines were

cultured at 37 °C in a 37 °C, 5% CO₂ incubator in DMEM medium (Gibco) with 10%(v/v) BCS (Sigma) and 1%(v/v) streptomycin/penicillin/gentamicin. Furthermore, the above cell lines were free of mycoplasma contamination and were passaged <10 times after being revived from frozen stock.

Plasmid constructs

The overexpression (OE) plasmid pEnter-LCAT was purchased from Vigene Biosciences (CH896503). Moreover, all constructions were confirmed by DNA sequencing. Subsequently, cells were transfected with the LCAT or vector plasmids using LipoMax DNA Transfection Reagent (SUDGEN, 32,110) according to the manufacturer's procedure to establish transduced cell lines. After transfection for 6 h, the medium was replaced with medium supplemented with 10% (v/v) BCS. After that, we verified the expression of LCAT in the cells via Western blotting.

Quantitative real-time PCR assays

As previously mentioned [16, 17], quantitative real-time PCR experiments were carried out. In brief, the PrimeScript™ RT Reagent Kit with gDNA Eraser (TaKaRa, Kusatsu, Japan) was used for reverse transcription after total RNA was extracted using RNAiso Plus (TaKaRa, Kusatsu, Japan) reagent. Afterward, real-time PCR was performed using a Bio-Rad CFX Connect real-time PCR apparatus. By deducting the Ct values of beta-actin (ACTB), the Ct values of each gene were normalized. Additional file 2: Table S2 contains a list of the primers.

Western blot analysis

The collected cells were washed twice with PBS buffer washed before being lysed with IP lysis buffer containing protease inhibitor cocktail for two hours on ice. The systems were set up after 15 min of centrifugation at 15,000 rpm to determine the supernatant (BCA protein assay). Total protein was isolated using SDS–polyacrylamide gel and then transferred to a polyvinylidene fluoride (PVDF) membrane. The membranes were incubated overnight with different primary antibodies at 4 °C, incubated with the corresponding secondary antibody for 2 h at room temperature, and exposed via the ChemiDox XRS+ image-forming system. The following antibodies were used: anti-LCAT (Baijia; IPB11128), and anti-β-actin (Sigma; cat #A5411).

Cell viability, colony formation and transwell assays

Cell proliferation, colony formation, and Transwell experiments were conducted, as previously reported [18]. In brief, the cell Counting Kit-8 (CCK-8) test was used for the cell viability experiment in accordance with the manufacturer's instructions (Bimake). First, 1000

cells were plated in 96-well plates with five parallel wells in each group. Next, 10 μL of CCK-8 reagent was added to each well at each time point (0 h, 24 h, 48 h, 72 h, 96 h), and each well was then incubated for 2 h at 37 °C with 5% CO₂ for 2 h, and the OD450 was detected (BioTek).

In addition, cells were seeded onto six-well plates at a density of 500 cells per well for the colony formation experiment, and the plates were then incubated for 2 weeks. Each cell was seeded with three parallel wells. Then, the cells were fixed with methanol for 10 min, stained with 0.5% crystal violet for 30 min and subsequently counted using a microscope and ImageJ software (1.47 v, NIH, USA).

In the Transwell migration assay, 5 × 10⁴ cells were plated in each 24 well chamber (8.0 μm pore size, Falcon) and incubated for 24 h. For the invasion test, 100 μl of Matrigel (Becton, Dickinson and Company, USA) was diluted 1:9 with serum-free media and placed onto transwell chambers. Each compartment received 1 × 10⁵ cells, which were then cultivated for 48 h later. After that, the cells were fixed with methanol, stained with 0.5% crystal violet for 30 min and examined under an optical microscope. Each of these assays was repeated at least three times.

Immunofluorescence analysis

Cells were placed on chamber slides and then were washed three times with PBS. Subsequently, they were permeabilized with 0.5% Triton X-100 (v/v) for 5 min at room temperature after fixation with 4% paraformaldehyde for ten min. For each slide, 100 nM Actin-stain™ 555 (Cytoskeleton, PHDH1) in PBS was added and incubated at RT for half an hour in the dark. Next, the slides were contained with DAPI for 10 min, and washed 3 times with PBS. Finally, a Zeiss LSM9 confocal microscope was used to capture fluorescence images.

Results

Development of disulfidptosis-regulated clusters and their features in HCC

We proceeded by analyzing the expression of DRG in the tumor tissues and adjacent tissues of TCGA cohort HCC cases. Except for NDUFS1, EPAS1 and NUBPL, the expression of the other 13 DRGs including NCKAP1, PPM1F, GYS1, NDUFC1, CNOT1, NDUFA10, LRP-PRC, SLC7A11, OXSM, NUDFS2, RPN1, SLC3A2 and NDUFA11, was significantly upregulated in HCC tissues (Fig. 2A). The frequency of CNVs in 16 DRGs from HCC was next examined; most DRGs showed copy number amplification and deletion (Fig. 2B). The locations of the CNV changes for 16 DRGs on 23 chromosomes are shown in Fig. 2C. We classified HCC patients in the TCGA dataset using a consensus clustering approach in

order to further define the expression signatures of DRG in HCC patients. The clustering results showed that when $k=2$ was optimal (Additional file 1: Figure S1A–F), and these patients were well divided into two clusters (165 in Cluster 1, 200 patients in Cluster 2). Using ESTIMATE algorithms to evaluate the immune infiltration of the two clusters, we found that compared to cluster 2, cluster 1 had a higher immune score, suggesting the potential immune regulation function of DRGs in HCC (Fig. 2D). Then, the Kaplan–Meier analysis showed that patients in Cluster 1 had a lower overall survival (OS) rate and a shorter progression-free interval (PFI) than those in Cluster 2 (Fig. 2E, F).

Construction of the disulfidptosis-related prognostic model

We used the “limma” R package to analyze the differences in gene expression between the two clusters. A total of 373 DEGs were screened out, and after further using univariate Cox regression analysis to select those genes with prognostic significance, a total of 190 DEGs were included in the following analysis (Additional file 2: Tables S3, S4). The majority of metabolism-related pathways, including those for amino acid metabolism and fatty acid metabolism, were repressed in Cluster 1 according to GSEA of hallmark pathways, KEGG pathway analysis, and GO enrichment analysis based on the DEGs (Additional file 1: Figure S2A–C). On the other hand, immune-related pathways, such as the inflammatory response and TNF- α signaling via the NF- κ B pathway, were activated in Cluster 1, suggesting differences in immune status and metabolism regulation between these two disulfidptosis clusters. The best λ value was then determined using LASSO regression analysis, and 19 hub genes were determined (Fig. 3A, B). Among these hub genes, LCAT, TRIM55, GHR, OGN, TCP10L and DNASE1L3 were identified as protective genes, while GAGE1, PPP2R2C, TNFRSF11B, IL8, TREM1, SLC2A1, SCIN, AKR1B15, MMP1, CORIN, SLC1A5, GAGE4 and NEIL3 were identified as risk-related genes (Fig. 3C). The volcano plot showed that all the risk genes were significantly upregulated and the protective genes were significantly downregulated in Cluster 1 (Fig. 3D). The results of the univariate analysis indicated the adverse or protective effects of these hub genes on patient survival in Cluster 1 (Fig. 3E). Then, we constructed the disulfidptosis-related gene score model based on the LASSO regression results: DRG score = $(-0.05847) \times \text{LCAT} + (-0.02276) \times \text{TRIM55} + (-0.02275) \times \text{GHR} + (-0.01317) \times \text{OGN} + (-0.01217) \times \text{TCP10L} + (-0.0027) \times \text{DNASE1L3} + 0.00039 \times \text{GAGE1} + 0.0009 \times \text{PPP2R2C} + 0.00413 \times \text{TNFRSF11B} + 0.00576 \times \text{IL8} + 0.00878 \times \text{TREM1} + 0.01065 \times$

$\text{SLC2A1} + 0.01942 \times \text{SCIN} + 0.02512 \times \text{AKR1B15} + 0.02715 \times \text{MMP1} + 0.03276 \times \text{CORIN} + 0.0385 \times \text{SLC1A5} + 0.0627 \times \text{GAGE4} + 0.06288 \times \text{NEIL3}$. In the TCGA-LIHC training cohort, patients with high a DRG score had a substantially worse survival rate (Fig. 3F, G). In the training cohort, the DRG score had satisfactory predictive value (AUC for survival at 1 year, 3 years, and 5 years were 0.787, 0.748, and 0.711, respectively; Fig. 3H).

Validation of the prognostic model and establishment of a disulfidptosis-related predictive nomogram for HCC

Next, we chose the ICGC-LIRI-JP liver cancer cohort as our test cohort to validate our prognostic model. Similar to our previous analysis, with the increase in DRG score, the risk of patient death increased, and the survival time decreased. K–M survival curves revealed that the high DRG score group had poorer overall survival (Fig. 4A, B). Importantly, the one-year and three-year survival predictions based on the DRG score model had AUC values of 0.674 and 0.741, respectively, in the ICGC-LIRI-JP validation cohort (Fig. 4C). Then, we performed multivariate Cox regression analyses on the clinical characteristics of the TCGA-LIHC cohort and the DRG score and found that DRG score and stage can be used as independent prognostic predictors for HCC patients (Fig. 4D). We further integrated the DRG score and stage to create a nomogram in the TCGA-LIHC cohort to create individualized predictions for HCC patients (Fig. 4E). Furthermore, the nomogram model’s AUC value for patient OS accuracy was better (AUC for 1 year, 3 years, and 5 years of survival were 0.806, 0.758, and 0.730, respectively; Fig. 4F). Importantly, compared with stage or DRG score alone, the nomogram model showed higher predictive value for patient survival status (Fig. 4G, H). The DCA curve also suggested that the nomogram model performs better in clinical practice than stage or DRG score alone (Fig. 4I).

Evaluation of tumor microenvironment features based on the DRG scores

We initially employed ESTIMATE methods to compare the immune infiltration features of the two patient groups with high and low DRG scores in order to better understand the characteristics of the immunological milieu of the two patient groups. Patients with high and low DRG scores had significantly different immune scores (Fig. 5A). Using the CIBERSORT method, we further examined the relationship between 19 hub genes and different immune cells and found that the expression of these genes in the TCGA-LIHC cohort was closely related to the infiltration levels of macrophages, NK cells and T cells (Fig. 5B). Moreover, we

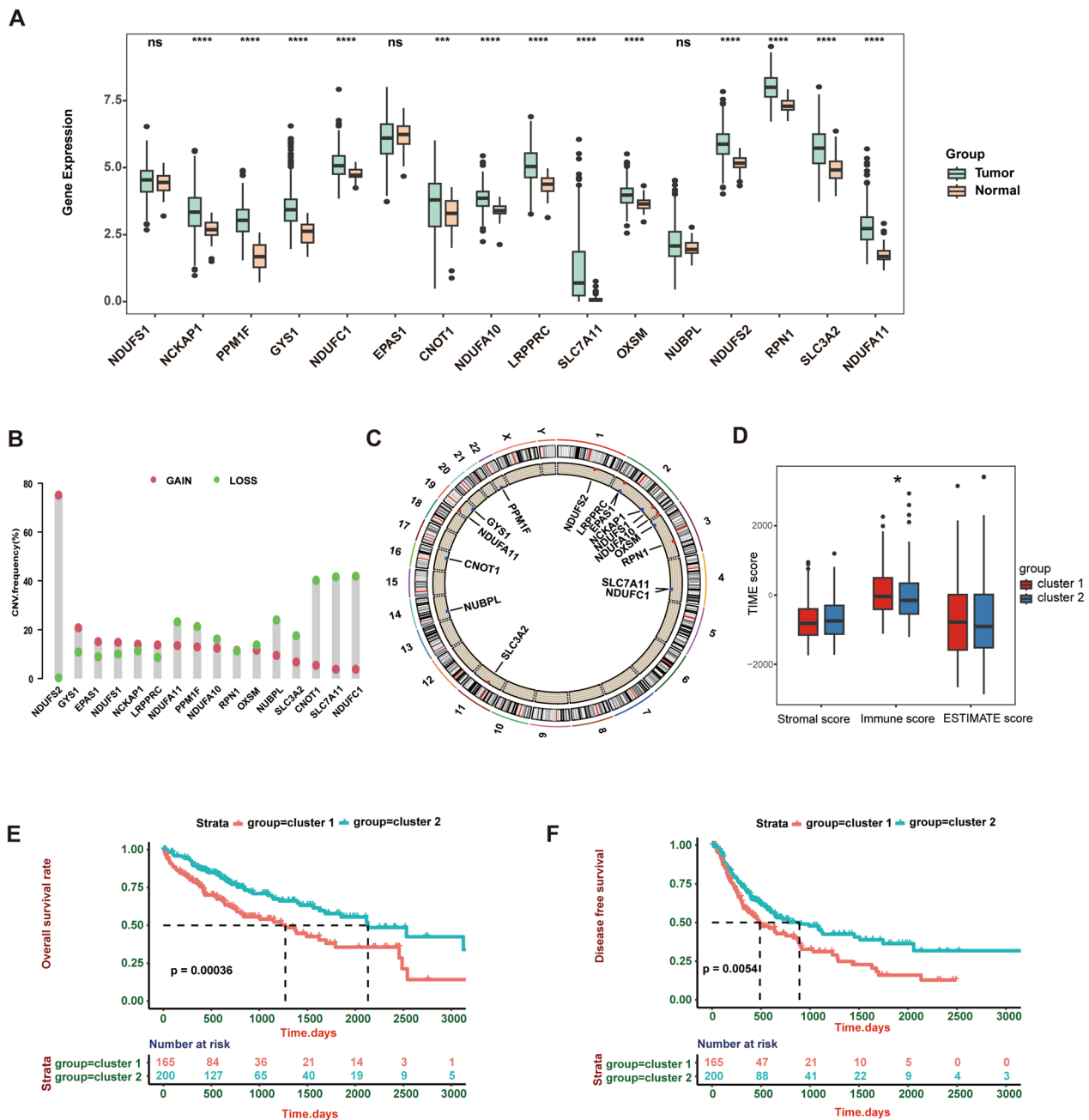


Fig. 2 Identification of disulfidptosis-regulated clusters based on 16 DRGs in HCC. **A** Differences in the expression levels of 16 DRGs in HCC and normal tissue, most of those genes were significantly upregulated in HCC tissues. **B** CNV (amplification and deletion) frequencies of DRGs in HCC. **C** The location of CNVs of DRGs on 23 chromosomes. **D** Boxplot showing the significant difference in the immune score between the two disulfidptosis-regulated clusters in the TCGA cohort (Wilcoxon test, $* P < 0.05$). **E** and **F** The prognosis analysis for two disulfidptosis-regulated clusters: Cluster 1 had lower overall survival (OS) and progression-free interval (PFI) than Cluster 2. P values are shown as $*$ $P < 0.05$; $** P < 0.01$; $*** P < 0.001$; ns, not significant. DRGs Disulfidptosis-related genes, HCC hepatocellular carcinoma, CNV copy number variation, OS overall survival, PFI progression-free interval, TIME tumor immune microenvironment

also found that in the high DRG score group, the infiltration levels of macrophages and Tregs were higher, while the infiltration levels of naive B cells, CD4+ T cells and CD8+ T cells were lower (Fig. 5C), suggesting

that the high DRG score group had a suppressive immune microenvironment, which coincided with their poorer overall survival outcomes. In addition, we analyzed the correlation between the expression of

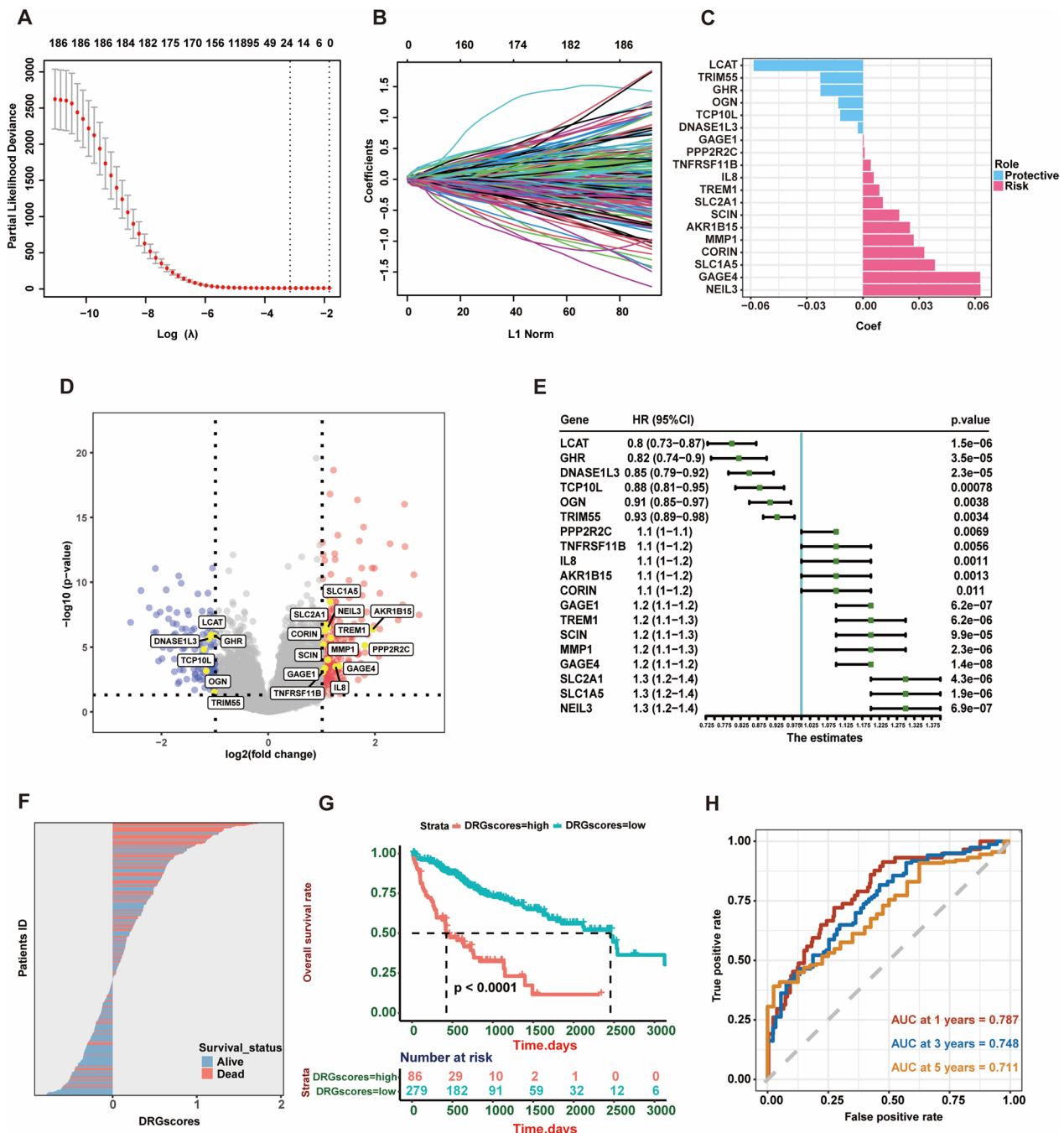


Fig. 3 Construction of the disulfidptosis-related prognostic model in HCC. **A** and **B** LASSO regression identified hub DRGs and coefficient profiles. **C** Histogram showing the 6 protective genes and 13 risk genes and their weighted coefficients. **D** Volcano plot of 19 selected hub genes between two disulfidptosis-regulated clusters. **E** Univariate Cox regression analysis of selected hub genes associated with overall survival in HCC patients. **F** Distribution of DRG scores and patient survival status in the TCGA-LIHC cohort. **G** and **H** The Kaplan–Meier OS curves **G** and time-dependent ROC curves **H** for patients in the high- and low-DRG score groups in the TCGA training cohort. The group with high DRG scores had worse survival rates, and the AUC values of DRG scores for one-year, three-year, and 5 year OS were 0.787, 0.748, and 0.711, respectively. DRGs Disulfidptosis-related genes; HCC hepatocellular carcinoma, LASSO least absolute shrinkage and selection operator, DEGs differentially expressed genes, LIHC liver cancer, ROC receiver operating characteristic

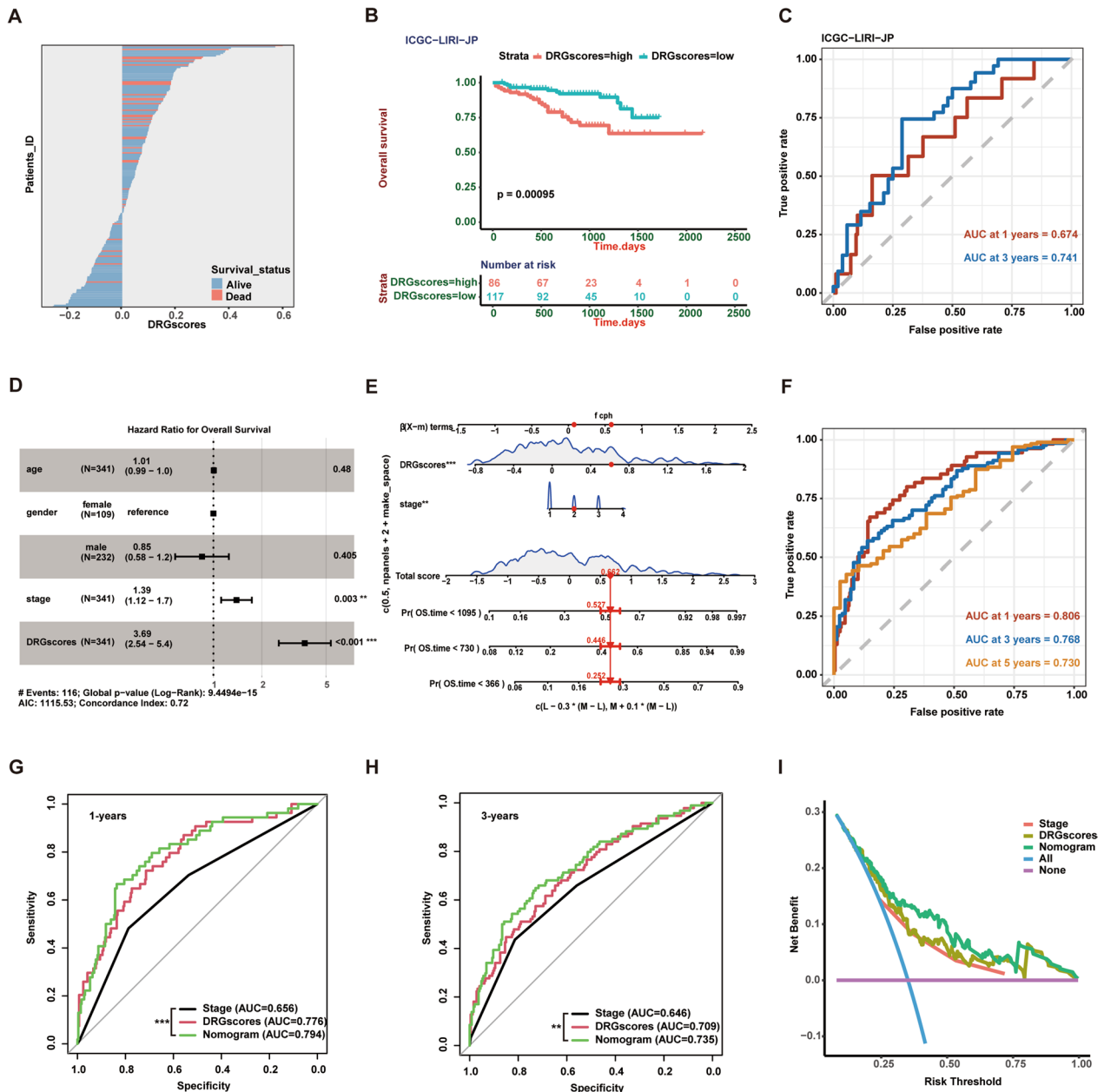


Fig. 4 Validation of the DRG score model and establishment of a disulfidptosis predictive nomogram for HCC. **A–C** Distribution of patient survival status **A** and Kaplan–Meier OS curves **B** and time-dependent ROC curves **C** for patients in the high- and low-DRG score groups in the ICGC–LIRI-JP validation cohort. The group with high DRG scores had a worse survival rates ($P = 0.00095$), and the AUC values of the DRG scores for 1 year and 3 year OS were 0.674 and 0.741, respectively. **D** Multivariate Cox regression showed that high stage ($P = 0.003$, HR = 1.39) and DRG score ($P < 0.001$, HR = 3.69) were independent risk factors for worse OS. **E** The establishment of a nomogram to predict the 1-, 3-, and 5 year overall survival probability for HCC patients in the TCGA cohort. **F** The ROC curves demonstrated that the nomogram model's AUC values for one-year OS, 3 year OS, and 5 year OS were 0.806, 0.768, and 0.730, respectively. **G** and **H** Compared with stage or DRG score alone, the nomogram model showed a higher AUC value for 1 year **G** and three-year **H** OS, which suggested that the model was effective. **I** The DCA curve suggested that the nomogram model performs better in clinical practice than stage or DRG score alone. P values are shown as * $P < 0.05$; ** $P < 0.01$; *** $P < 0.001$; ns not significant. DRGs Disulfidptosis-related genes, ROC receiver operating characteristic, ICGC international cancer genome consortium, HCC hepatocellular carcinoma, AUC area under curve, DCA decision curve analysis

immune checkpoint genes (CD274, PDCD1, CTLA4, CD276, HAVCR2, TIGIT and IDO1) and DRG score in the TCGA-LIHC cohort [19, 20]. We observed a significant positive correlation between the immune checkpoint genes and DRG score (Fig. 5D–J). Analysis of the features of hub genes at the single-cell level to better understand the effectiveness of the constructed model has become a commonly employed method in recent years [21]. We analyzed the single-cell data of untreated hepatitis B virus (HBV)-related hepatocellular carcinoma (HCC) patients (GSE202642) [15]. Following the study conducted by Zhu et al., 9 cell clusters were identified (Additional file 1: Figure S3A, B). Subsequently, we investigated the expression of our hub DRGs within each cell cluster. The results indicated that the DRG signature was predominantly distributed on tumor cells, endothelial cells, cancer-associated fibroblasts (CAFs), tumor-associated macrophages (TAMs), and T cells, which corresponded to our CIBERSORT immune infiltration analysis results.

Correlations of the DRG scores with immunotherapy and drug sensitivity

We then applied the TIDE algorithm to evaluate the immunotherapy response for HCC patients in the TCGA-LIHC cohort. According to our results (Fig. 6A, B), patients with low DRG scores may benefit more from immunotherapy because their TIDE scores were significantly higher than those of the low DRG score group and their response rates were significantly lower than those of the high DRG score group. We further predicted the efficacy of 198 drugs by the oncoPredict R package in TCGA-LIHC and assessed the drug sensitivity of the high- and low-DRG score groups. Forty drugs were negatively correlated with DRG scores ($P < -0.2$, Additional file 2: Table S5), and Fig. 6C shows the top ten drugs with a negative correlation. Chemotherapy drugs for liver cancer, such as cisplatin and vinorelbine, and the targeted drugs gefitinib and sorafenib had lower IC50 values in patients with high DRG scores (Fig. 6D–G), suggesting that the above drugs have better therapeutic effects on these patients. Overall, the

findings showed that the prognostic model based on DRG scores can aid in predicting the efficacy of medications in HCC patients.

Validation of the DRG hub genes in HCC cell lines and functional analysis

We initially used qPCR to assess the mRNA expression levels of hub DRGs in two liver cancer cell lines (HepG2 and Hep3B) and a normal liver cell line (L-02) to further validate our investigation. The results demonstrated that LCAT and DNASE1L3 were significantly downregulated in liver cancer cells, while NEIL3, GAGE4, SLC1A5, MMP1, SCIN and GAGE1 mRNA expression levels were notably elevated (Fig. 7A), in agreement with the bioinformatics prognostic model described above. The mRNA expression levels of a few hub genes were too low in the liver cancer cell line to be detected by qPCR. Since the protective gene LCAT has the lowest risk coefficient for hepatocellular carcinoma, we further explored the expression profile and identified the biological function of LCAT. Firstly, Western blotting analysis revealed that liver cancer cells expressed less of the LCAT protein than normal liver cells did (Fig. 7B, Additional file 1: Fig. S4A). After that, to examine the impact of LCAT overexpression in HCC, we established LCAT overexpressing HCCLM3 and Hep3B cell lines (Fig. 7C, Additional file 1: Figure S4B, C). Transwell assays indicated that increasing LCAT expression dramatically reduced the capacity of LM3 and Hep3B cells to migrate and invade (Fig. 7D, E). However, LCAT did little to suppress the cell proliferation (Additional file 1: Fig. S4D, E) and colony formation (Additional file 1: Fig. S4F, G) capabilities of liver cancer cells in vitro. Thus, we inferred that LCAT is primarily associated with liver cancer metastasis. Moreover, we treated LM3 cells with BAY-876 (Selleck, S8452), a GLUT1 inhibitor agent, to block glucose uptake. Immunofluorescence results showed that overexpressing LCAT in LM3 cells during glucose deprivation obviously altered their cell shape, including F-actin contraction and cell shrinkage (Fig. 7F). Furthermore, the reducing drug TCEP (Selleck, S4611) was successful in preventing disulfidptosis-induced cell death. Hence, LCAT enhanced glucose starvation-induced disulfidptosis of liver cancer

(See figure on next page.)

Fig. 5 Evaluation of tumor microenvironment (TME) features based on the DRG score. **A** Boxplot showing that the immune score of the high-DRG group was significantly higher than that of the low-DRG score group in the TCGA cohort (Wilcoxon test, *** $P < 0.001$). **B** CIBERSORT analysis of correlations between the proportion of immune cells and 19 hub genes showed that these genes in HCC patients in the TCGA cohort were closely related to macrophages, B cells, NK cells and T cells. **C** Boxplot showing the proportion of immune cells in the low- and high-DRG score groups in HCC patients, which suggested that the high DRG score group had higher infiltration levels of macrophages and Tregs and lower infiltration levels of naive B cells, CD4+T cells and CD8+T cells. **D–J** The immune checkpoint genes (CD274, PDCD1, CTLA4, CD276, HAVCR2, TIGIT and IDO1) significantly correlated with the DRG score. P values are shown as * $P < 0.05$; ** $P < 0.01$; *** $P < 0.001$; ns, not significant. *HCC* hepatocellular carcinoma, *TME* tumor microenvironment, *DRGs* Disulfidptosis-related genes

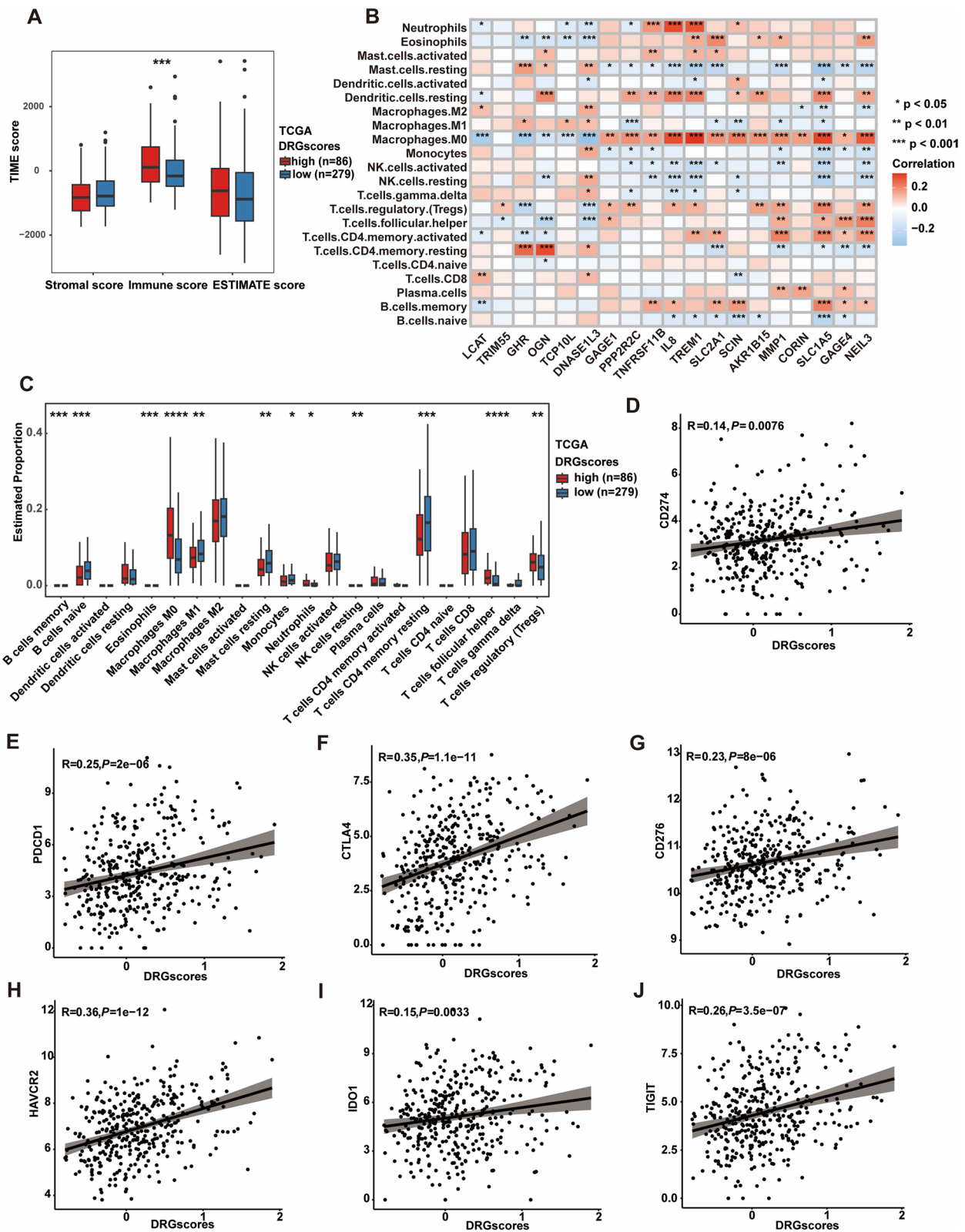


Fig. 5 (See legend on previous page.)

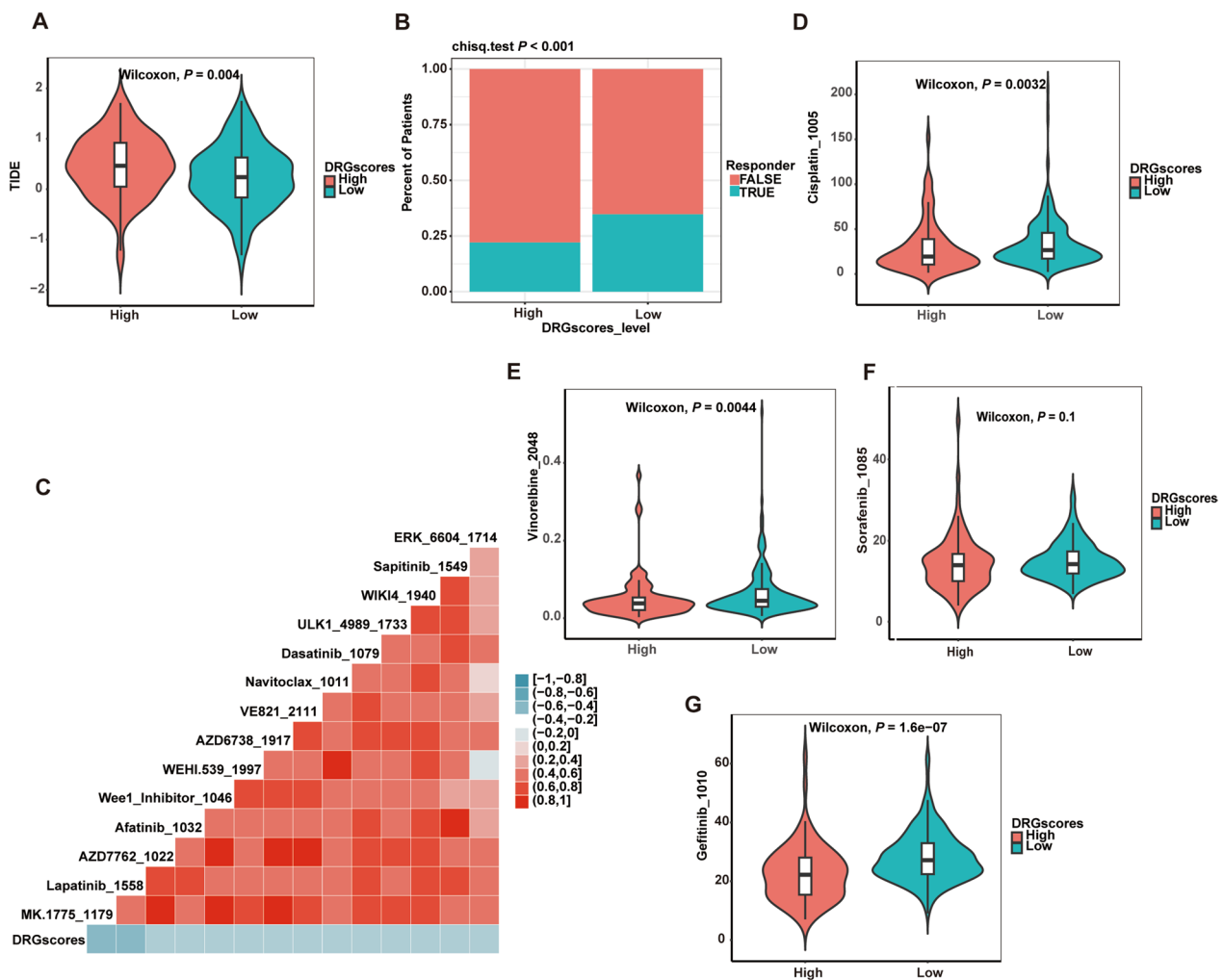


Fig. 6 Correlations of the DRG score with immunotherapy and chemotherapeutic sensitivity in HCC. **A** Compared to patients in TCGA-LIHC with low DRG scores, those in the high DRG score group exhibited higher TIDE scores (Wilcoxon, $P < 0.01$). **B** The response rate of the high DRG score group was significantly lower than that of the low DRG score group (chi sq. test $P < 0.001$). **C** Correlations of the DRG scores and drug sensitivity in patients (Spearman correlation < -0.2). The therapeutic sensitivity of cisplatin **D**, vinorelbine **E**, sorafenib **F**, and gefitinib **G** between the high- and low-risk groups. *DRGs* Disulfidptosis-related genes, *TIDE* Tumor immune dysfunction and exclusion

cells through actin cytoskeletal network breakdown. Finally, we analyzed the expression differences of LCAT in HCC patient tumor tissues and adjacent nontumor tissues in TCGA. Then, we generated the survival curves for patients with high LCAT expression ($n = 240$) and low LCAT expression ($n = 123$). The results revealed a significantly lower expression of LCAT in cancer tissues than

in adjacent nontumor tissues (Fig. 7G). Furthermore, patients with high LCAT expression exhibited a better survival status (Fig. 7H). These findings also suggest that LCAT may serve as a protective gene, suppressing the progression of liver cancer. Our findings collectively suggest that LCAT slows the progression of HCC by mediating disulfidptosis.

(See figure on next page.)

Fig. 7 Validation of the hub DRGs in HCC cell lines and functional analysis. **A** qPCR was used to analyze the mRNA expression of the protective and risk-related genes for disulfidptosis model in liver cancer cells. **B** Western blotting analyses of LCAT expression in liver cancer cell lines. **C** Western blotting analyses of LCAT expression in LM3 and Hep3B cell lines. **D** Migration was measured in LCAT-overexpressing LM3 and Hep3B cells. **E** Invasion was measured in LCAT-overexpressing LM3 and Hep3B cells. **F** Fluorescence staining of F-actin with phalloidin in vector and *LCAT*-OE LM3 cells treated with 5 μM BAY-876 or 1 mM TCEP for 18 h. **G** and **H**: The expression of LCAT in tumor tissues was significantly lower than that in adjacent nontumor tissues in HCC patients in the TCGA cohort **G**, and patients with higher LCAT expression demonstrated better survival outcomes **H**

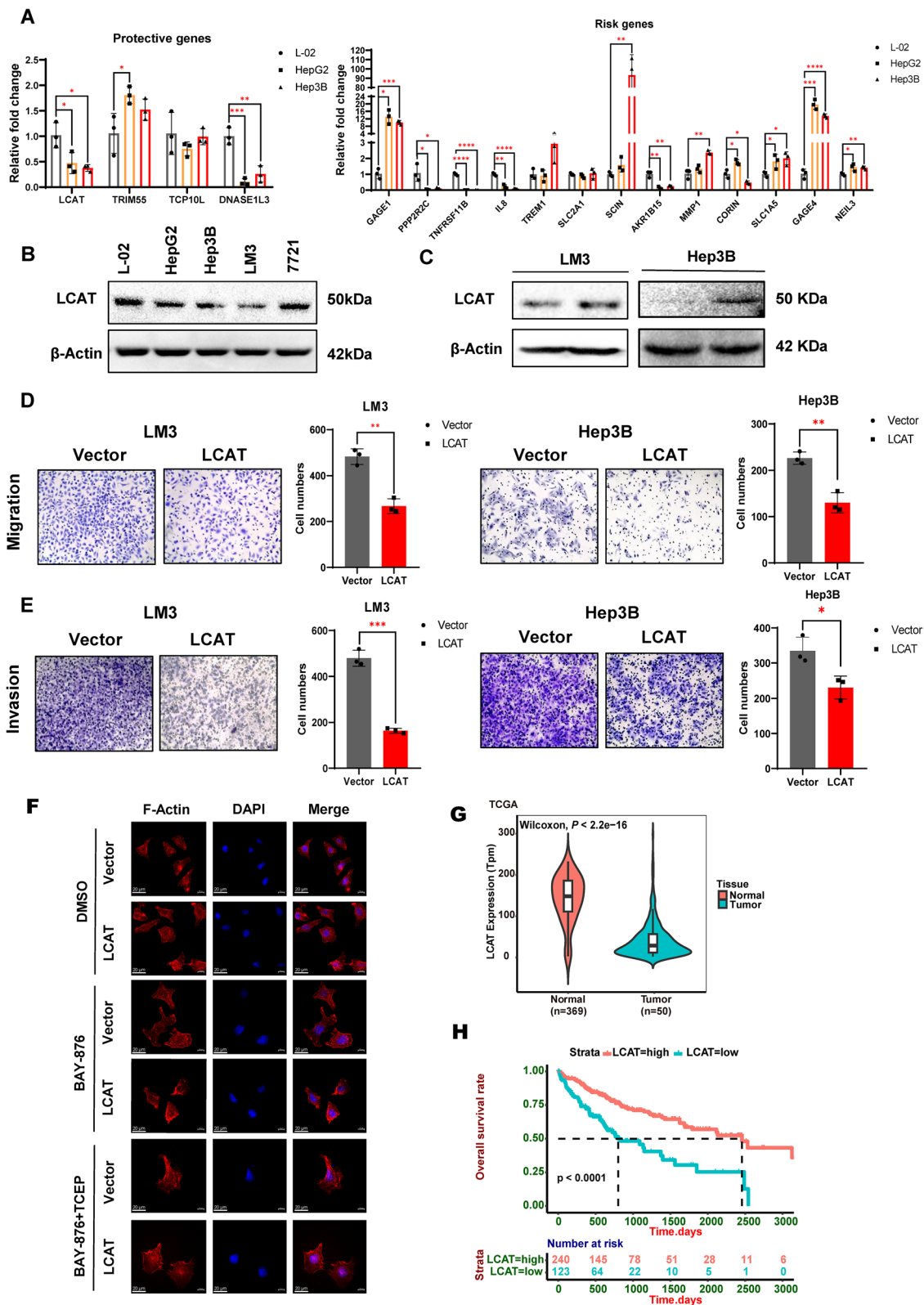


Fig. 7 (See legend on previous page.)

Discussion

Disulfidptosis, as a newly discovered form of PCD, is closely associated with cancer metabolism and provides new insights for cancer treatment. However, the specific role of this cell death pathway in various types of tumors remains poorly understood, and its relationship with hepatocellular carcinoma (HCC) is still unclear.

In our research, we selected 16 genes critical for mediating and inhibiting the occurrence of disulfidptosis as disulfidptosis-related genes. Considering that disulfidptosis is an induced process in cancer cells, analysis of genes involved in this process could accurately and fundamentally reflect the disulfidptosis status of each patient, and our data support the reliability of the model. From the DRGs, we identified 19 hub genes to construct our model. Among these genes, 6 genes were identified as protective genes and the remaining 13 genes were identified as risk-related genes. Importantly, we validated the expression of some genes in liver cancer and normal liver tissue cell lines through RT-qPCR experiments.

We further selected lecithin-cholesterol acyltransferase (LCAT) for biological functional experiments. LCAT is involved in cholesterol transport and converts free cholesterol into its hydrophobic form, ultimately synthesizing high-density lipoprotein (HDL) [22]. LCAT is abundantly expressed in the human body and has low expression in breast cancer and liver cancer tissue that in compared to normal tissue, but high expression in the serum of advanced breast cancer, suggesting that LCAT may serve as a plasma protein biomarker for late-stage breast cancer and metastasis [23]. In contrast, LCAT levels are lower in the serum of colorectal cancer, liver cancer, and ovarian cancer patients, making it a potential biomarker [24–26].

In addition, bioinformatics analysis has indicated that LCAT plays a critical role in the development of liver cirrhosis into HCC [27]. Our experiments have confirmed the low expression of LCAT in liver cancer cell lines, consistent with previous reports [28]. Furthermore, *in vitro* experiments have clearly demonstrated that LCAT significantly inhibits the migration and invasion abilities of liver cancer cells, and promotes cell death via disulfide bond formation under glucose deprivation conditions. However, LCAT has a limited impact on the proliferation and colony formation abilities of liver cancer cells, suggesting that LCAT mainly affects the metastasis of liver cancer by inducing disulfidptosis. Then, the role of LCAT in disulfidptosis need further experimental verification. Since LCAT is a newly discovered tumor suppressor, it is worthwhile to further investigate the molecular mechanisms by which LCAT affects disulfidptosis in HCC.

Moreover, our results demonstrated that the developed DRG score model successfully divides HCC patients

into two clusters. The group with high DRG scores had a worse prognosis and exhibited an immunosuppressive microenvironment characterized by immune infiltration. Additionally, this group showed stronger resistance to immune therapy. However, these patients demonstrated greater sensitivity to certain chemotherapy drugs for liver cancer, such as cisplatin and vinorelbine. Immune cells, particularly CD4+T cells, CD8+T cells, and Th cells, play critical roles in a variety of diseases, including cancer and several infectious diseases [29–31], and some costimulatory molecule and immune check point such as CD40 and PD-1 are extensively expressed abnormally in different immune cells [32, 33]. In our study, CIBERSORT analysis showed that DRG hub genes are closely related to T cells. Patients with high DRG scores have lower CD4+T cell and CD8+T infiltration, and DRG scores are positively correlated with the expression of immune checkpoint genes such as PD-1. These results also suggested that patients with high DRG scores may be more sensitive to immunotherapy.

Currently, sorafenib, which targets ferroptosis in liver cancer cells, is the most useful first-line chemotherapy drug for the treatment of advanced HCC [34, 35]. Moreover, regulating ferroptosis could also alleviate the tumor immunosuppressive microenvironment, thereby enhancing the sensitivity of patients to immunotherapy [36]. In addition, applying AEG35156, resminostat (4SC-201) or panobinostat (LBH589) induced apoptosis in patients with HCC [37]. Since some patients present drug resistance, exploring other effective therapeutic approaches for hepatic carcinoma is still a great challenge [38]. Thus, treating liver cancer patients by promoting disulfidptosis is a potential way to improve patient survival.

It must be noted out that our research has certain limitations. First, the data used to construct and validate the model were derived solely from public databases, which may not fully reflect the characteristics and conditions of all HCC patients. Second, we selected 16 genes involved in the mechanism of disulfidptosis, of which only a portion have been validated, while some are potential mediators of disulfidptosis. As the investigation into the mechanism of disulfidptosis progresses, the effectiveness of the model we constructed can be further confirmed. Third, it demands more robust assays to explore the molecular mechanisms by which LCAT induces disulfidptosis, and to demonstrate that LCAT is capable of hindering liver cancer metastasis. Moreover, other hub genes of disulfidptosis besides LCAT deserve additional in-depth study. Overall, the DRG score model links disulfidptosis to hepatocellular carcinoma, and could be used for survival prognosis prediction in HCC patients; it provides valuable assistance for personalized treatment approaches.

Supplementary Information

The online version contains supplementary material available at <https://doi.org/10.1186/s12935-023-03188-y>.

Additional file 1: Figure S1. Consensus cluster analysis of HCC patients based on disulfidptosis-regulated genes. **A and B** The cumulative distribution function (CDF) and relative change in the area under the CDF curve when k takes different values. **C–F** The diagrams show consistent clustering results when k was 2, 3, 4, and 5. It was most reliable when k was 2. **Figure S2.** The GSEA results of Hallmark pathway and KEGG pathway and GO enrichment analysis base on two DRGs clusters. **Figure S3.** Distribution of hub DRGs at the single-cell level. **(A and B)** UMAP plots of GSE202642 and different cell clusters were identified and visualized. **C** Expression of the DRG signature in 9 cell types. **Figure S4.** Biological function analysis of liver cancer cells overexpressing LCAT. **A** Related LCAT expression in liver cancer cells and normal liver cells. **B** Related LCAT expression in LM3 cells that overexpressed LCAT. **C** Related LCAT expression in overexpression LCAT Hep3B cells. **D and E** The CCK-8 assay was performed to assess the viability of LM3 and Hep3B cells overexpressing LCAT. **F and G** A plate colony formation assay was performed in LM3 and Hep3B cells that were transfected with LCAT.

Additional file 2: Table S1. The details of selected 16 disulfidptosis-related genes. **Table S2.** Primers for RT-PCR **Table S3.** 373 differential expression genes between two disulfidptosis-related clusters. **Table S4.** 190 differential expression genes with prognostic significance. **Table S5.** The correlations between the DRGs scores and the sensitivity of 198 drugs in HCC patients.

Acknowledgements

Thanks for all the members who conducted the experiments and manuscript.

Author contributions

SL, TY and TJ conceived the study; TJ, SL and PX completed the data analysis and experimental parts; TJ and PX wrote the manuscript; TY, LS AND XD reviewed the manuscript.

Funding

This work was supported by the National Natural Science Foundation of China [82272982, 82072594, 82073097, 81874139 and 82073136], Hunan Provincial Key Area R&D Programs [2019SK2253 and 2021SK2013], the Science and Technology Innovation Program of Hunan Province [2022RC3072], and the Central South University Research Program of Advanced Interdisciplinary Studies [2023QYJC030].

Availability of data and materials

Please contact the corresponding author for all data requests.

Declarations

Ethics approval and consent to participate

The Central South University Health Authority's Joint Ethics Committee evaluated, approved, and ensured that all protocols were carried out in conformity with federal regulations.

Consent for publication

The publishing of the manuscript was approved by all authors.

Competing interests

The authors claim to have no competing interests. The authors say they have no competing interests. All authors have read and approved the work, which is not currently being considered for publication elsewhere.

Received: 13 September 2023 Accepted: 21 December 2023

Published online: 09 January 2024

References

- Anwanwan D, Singh SK, Singh S, Saikam V, Singh R. Challenges in liver cancer and possible treatment approaches. *Biochim Biophys Acta Rev Cancer*. 2020;1873(1): 1883–14.
- Li X, Ramadori P, Pfister D, Seehawer M, Zender L, Heikenwalder M. The immunological and metabolic landscape in primary and metastatic liver cancer. *Nat Rev Cancer*. 2021;21(9):541–57.
- Zheng Y, Wang S, Cai J, Ke A, Fan J. The progress of immune checkpoint therapy in primary liver cancer. *Biochim Biophys Acta Rev Cancer*. 2021;1876(2): 188638.
- Heinrich S, Craig AJ, Ma L, Heinrich B, Greten TF, Wang XW. Understanding tumour cell heterogeneity and its implication for immunotherapy in liver cancer using single-cell analysis. *J Hepatol*. 2021;74(3):700–15.
- Liu X, Nie L, Zhang Y, Yan Y, Wang C, Colic M, Olszewski K, Horbath A, Chen X, Lei G, et al. Actin cytoskeleton vulnerability to disulfide stress mediates disulfidptosis. *Nat Cell Biol*. 2023;25(3):404–14.
- Liu X, Olszewski K, Zhang Y, Lim EW, Shi J, Zhang X, Zhang J, Lee H, Koppula P, Lei G, et al. Cystine transporter regulation of pentose phosphate pathway dependency and disulfide stress exposes a targetable metabolic vulnerability in cancer. *Nat Cell Biol*. 2020;22(4):476–86.
- Machesky LM. Deadly actin collapse by disulfidptosis. *Nat Cell Biol*. 2023;25(3):375–6.
- Zheng P, Zhou C, Ding Y, Duan S. Disulfidptosis: a new target for metabolic cancer therapy. *J Exp Clin Cancer Res*. 2023;42(1):103.
- Chouhan S, Sawant M, Weimholt C, Luo J, Sprung RW, Terrado M, Mueller DM, Earp HS, Mahajan NP. TNK2/ACK1-mediated phosphorylation of ATP5F1A (ATP synthase F1 subunit alpha) selectively augments survival of prostate cancer while engendering mitochondrial vulnerability. *Autophagy*. 2023;19(3):1000–25.
- Liu Q, Li J, Zhang W, Xiao C, Zhang S, Nian C, Li J, Su D, Chen L, Zhao Q, et al. Glycogen accumulation and phase separation drives liver tumor initiation. *Cell*. 2021;184(22):5559–5576.e5519.
- Yu G, Wang LG, Han Y, He QY. clusterProfiler: an R package for comparing biological themes among gene clusters. *OMICS*. 2012;16(5):284–7.
- Iasonos A, Schrag D, Raj GV, Panageas KS. How to build and interpret a nomogram for cancer prognosis. *J Clin Oncol*. 2008;26(8):1364–70.
- Newman AM, Liu CL, Green MR, Gentles AJ, Feng W, Xu Y, Hoang CD, Diehn M, Alizadeh AA. Robust enumeration of cell subsets from tissue expression profiles. *Nat Methods*. 2015;12(5):453–7.
- Maeser D, Gruener RF, Huang RS. oncoPredict: an R package for predicting in vivo or cancer patient drug response and biomarkers from cell line screening data. *Brief Bioinform*. 2021. <https://doi.org/10.1093/bib/bbab260>.
- Zhu G-Q, Tang Z, Huang R, Qu W-F, Fang Y, Yang R, Tao C-Y, Gao J, Wu X-L, Sun H-X, et al. CD36+ cancer-associated fibroblasts provide immunosuppressive microenvironment for hepatocellular carcinoma via secretion of macrophage migration inhibitory factor. *Cell Discovery*. 2023;9(1):25.
- Wang M, Mao C, Ouyang L, Liu Y, Lai W, Liu N, Shi Y, Chen L, Xiao D, Yu F, et al. Long noncoding RNA LINC00336 inhibits ferroptosis in lung cancer by functioning as a competing endogenous RNA. *Cell Death Differ*. 2019;26(11):2329–43.
- Chen L, Cai Q, Yang R, Wang H, Ling H, Li T, Liu N, Wang Z, Sun J, Tao T, et al. GINS4 suppresses ferroptosis by antagonizing p53 acetylation with Snail. *Proc Natl Acad Sci USA*. 2023;120(15): e2219585120.
- Long Y, Guo J, Chen J, Sun J, Wang H, Peng X, Wang Z, Lai W, Liu N, Shu L, et al. GPR162 activates STING dependent DNA damage pathway as a novel tumor suppressor and radiation sensitizer. *Signal Transduct Target Ther*. 2023;8(1):48.
- Kalbasi A, Ribas A. Tumour-intrinsic resistance to immune checkpoint blockade. *Nat Rev Immunol*. 2020;20(1):25–39.
- Morad G, Helmink BA, Sharma P, Wargo JA. Hallmarks of response, resistance, and toxicity to immune checkpoint blockade. *Cell*. 2022;185(3):576.
- Ni LA, Yang HZ, Wu XY, Zhou KJ, Wang S. The expression and prognostic value of disulfidptosis progress in lung adenocarcinoma. *Aging-US*. 2023;15(15):7741–59.
- Dobiasova M, Frohlich JJ. Advances in understanding of the role of lecithin cholesterol acyltransferase (LCAT) in cholesterol transport. *Clin Chim Acta*. 1999;286(1–2):257–71.
- Park HM, Kim H, Kim DW, Yoon JH, Kim BG, Cho JY. Common plasma protein marker LCAT in aggressive human breast cancer and canine mammary tumor. *BMB Rep*. 2020;53(12):664–9.

24. Mihajlovic M, Gojkovic T, Vladimirov S, Miljkovic M, Stefanovic A, Vekic J, Zeljkovic D, Trifunovic B, Kotur-Stevuljevic J, Spasojevic-Kalimanovska V, et al. Changes in lecithin: cholesterol acyltransferase, cholesteryl ester transfer protein and paraoxonase-1 activities in patients with colorectal cancer. *Clin Biochem*. 2019;63:32–8.
25. Russell MR, Graham C, D'Amato A, Gentry-Maharaj A, Ryan A, Kalsi JK, Ainsley C, Whetton AD, Menon U, Jacobs I, et al. A combined biomarker panel shows improved sensitivity for the early detection of ovarian cancer allowing the identification of the most aggressive type II tumours. *Br J Cancer*. 2017;117(5):666–74.
26. Zhang X, Liu X, Zhu K, Zhang X, Li N, Sun T, Fan S, Dai L, Zhang J. CD5L-associated gene analyses highlight the dysregulations, prognostic effects, immune associations, and drug-sensitivity predicative potentials of LCAT and CDC20 in hepatocellular carcinoma. *Cancer Cell Int*. 2022;22(1):393.
27. Jiang CH, Yuan X, Li JF, Xie YF, Zhang AZ, Wang XL, Yang L, Liu CX, Liang WH, Pang LJ, et al. Bioinformatics-based screening of key genes for transformation of liver cirrhosis to hepatocellular carcinoma. *J Transl Med*. 2020;18(1):40.
28. Long J, Chen P, Lin J, Bai Y, Yang X, Bian J, Lin Y, Wang D, Yang X, Zheng Y, et al. DNA methylation-driven genes for constructing diagnostic, prognostic, and recurrence models for hepatocellular carcinoma. *Theranostics*. 2019;9(24):7251–67.
29. Zhang X, Kiapour N, Kapoor S, Khan T, Thamilarasan M, Tao Y, Cohen S, Miller R, Sobel RA, Markovic-Plese S. IL-11 Induces encephalitogenic Th17 cells in multiple sclerosis and experimental autoimmune encephalomyelitis. *J Immunol*. 2019;203(5):1142–50.
30. Seyedsadr M, Wang Y, Elzoheiry M, Shree Gopal S, Jang S, Duran G, Chervoneva I, Kasimoglu E, Wrobel JA, Hwang D, et al. IL-11 induces NLRP3 inflammasome activation in monocytes and inflammatory cell migration to the central nervous system. *Proc Natl Acad Sci USA*. 2023;120(26): e2221007120.
31. Hisamuddin M, Rizvi I, Malik A, Nabi F, Hassan MN, Ali SM, Khan JM, Khan TH, Khan RH. Characterization of pH-induced conformational changes in recombinant DENV NS2B-NS3pro. *Int J Biol Macromol*. 2023;253(Pt 3): 126823.
32. Khan TH, Srivastava N, Srivastava A, Sareen A, Mathur RK, Chande AG, Musti KV, Roy S, Mukhopadhyaya R, Saha B. SHP-1 plays a crucial role in CD40 signaling reciprocity. *J Immunol*. 2014;193(7):3644–53.
33. Tarique M, Naz H, Suhail M, Turan A, Saini C, Muhammad N, Shankar H, Zughaihi TA, Khan TH, Khanna N, et al. Differential expression of programmed death 1 (PD-1) on various immune cells and its role in human leprosy. *Front Immunol*. 2023;14:1138145.
34. Chen J, Li X, Ge C, Min J, Wang F. The multifaceted role of ferroptosis in liver disease. *Cell Death Differ*. 2022;29(3):467–80.
35. Chouhan S, Singh S, Athavale D, Ramteke P, Vanuopadath M, Nair BG, Nair SS, Bhat MK. Sensitization of hepatocellular carcinoma cells towards doxorubicin and sorafenib is facilitated by glucosedeependent alterations in reactive oxygen species, P-glycoprotein and DKK4. *J Biosci*. 2020. <https://doi.org/10.1007/s12038-020-00065-y>.
36. Huang Y, Wang S, Ke A, Guo K. Ferroptosis and its interaction with tumor immune microenvironment in liver cancer. *Biochim Biophys Acta Rev Cancer*. 2023;1878(1): 188848.
37. Luedde T, Kaplowitz N, Schwabe RF. Cell death and cell death responses in liver disease: mechanisms and clinical relevance. *Gastroenterology*. 2014;147(4):765–783.e764.
38. Athavale D, Chouhan S, Pandey V, Mayengbam SS, Singh S, Bhat MK. Hepatocellular carcinoma-associated hypercholesterolemia: involvement of proprotein-convertase-subtilisin-kexin type-9 (PCSK9). *Cancer Metab*. 2018;6:16.

Publisher's Note

Springer Nature remains neutral with regard to jurisdictional claims in published maps and institutional affiliations.

Ready to submit your research? Choose BMC and benefit from:

- fast, convenient online submission
- thorough peer review by experienced researchers in your field
- rapid publication on acceptance
- support for research data, including large and complex data types
- gold Open Access which fosters wider collaboration and increased citations
- maximum visibility for your research: over 100M website views per year

At BMC, research is always in progress.

Learn more biomedcentral.com/submissions

